Energy Proceedings
Vol 35, 2023
ISSN 2004-2965

Transition-Metal-Selenides Based Aerogel for Highly Efficient Electrocatalytic Hydrogen Evolution and 5-hydroxymethylfurfural Oxidation

Hongchen Liu[1], Fan Yang[1,] , Zhengyang Chen[1], Jinxiu Qian[1], Jianfeng Wang[1] , Ni Wu[1] and Yongfeng Li[1,]

1 State Key Laboratory of Heavy Oil Processing, China University of Petroleum, Beijing, 102249, China

(*Corresponding Author: yangfan@cup.edu.cn (F. Yang), yfli@cup.edu.cn (Y.F. Li))

ABSTRACT

The excessive dependence and abuse of fossil energy promoted the development of clean and renewable energy. Green hydrogen, generated from the hydrogen evolution reaction (HER) of renewable energy water electrolysis, is considered as an ideal choice for future energy. However, the coupling anodic oxygen evolution reaction (OER) with high potential limits the efficiency of hydrogen production. Herein, a bifunctional Ni_2P-$NiSe_2$ heterostructure aerogel (Ni-P-Se aerogel) was constructed to boost HER and replace OER by 5-hydroxymethylfurfural oxidation reaction (HMFOR) to produce high-valued 2,5-furandicarboxylic acid (FDCA) with low operating voltage and high conversion. The $NiSe_2$ with cubic pyrite-type crystal structure was favor for anodic reconstruction, which allowed the effective generation of activated oxygen species and further promoted HMFOR. Moreover, the coupling of Ni_2P modulated the adsorption energy of OH- in HMFOR and enhanced the activity toward HER. Besides, the aerogel structure with porous network structure provides abundant active sites and mass-transfer pathways. Benefit from these advantages, the optimized Ni-P-Se aerogel exhibited high HER performance (68 mV at 10 $mA{\cdot}cm^{-2}$), low onset oxidation potential (1.30 V) and high Faradaic efficiency (97.4% at 1.40 V) of HMFOR. Compared to OER, the two-electrode system coupled with HMFOR had significantly increased current density at low operating voltage (102 $mA{\cdot}cm^{-2}$ increase at 1.50 V), proving the superiority of HMFOR as alternative anodic reaction This work offers an anticipated perspective of bifunctional electrocatalysts toward the combination of HER and organics oxidation.

Keywords: Hydrogen evolution reaction, 5-hydroxymethylfurfura oxidation reaction, Heterostructure, Aerogel, Electrocatalysis.

NONMENCLATURE

Abbreviations	
HER	Hydrogen Evolution Reaction
OER	Oxygen Evolution Reaction
HMF	5-hydroxymethylfurfural
FDCA	2,5-furandicarboxylic acid
DFF	2,5-Diformylfuran
FFCA	2-formyl-5-furancarboxylic acid
HMFCA	5-Hydroxymethyl-2-furan-carboxylic acid
HMFOR	5-hydroxymethylfurfural oxidation reaction
HPLC	High performance liquid chromatography

1. INTRODUCTION

The overuse of non-renewable fossil fuels and growing environmental pollution promoted the utilization of renewable and ecofriendly energy resources[1]. Green hydrogen, which is generated from electrochemical water splitting powered by clean energy, is considered as one of the best future energy sources[2,3]. However, the anodic oxygen evolution reaction (OER) is the deficiency of water splitting, which produces low value-added oxygen with high theoretical potential and energy requirement. Alternatively, exploiting novel anodic oxidation reactions with favorable kinetics and high value-added product to couple with cathodic hydrogen evolution reaction (HER) provide a chance to increase the efficiency and benefits of electrolysis system[4]. In particular, 5-hydroxymethylfurfural (HMF), a typical biomass-based platform compound, and its electrooxidation process have been extensively investigated due to the lower

This is a paper for International CCUS Conference 2023 (ICCUSC2023), April 14-15, 2023, Beijing, China.

theoretical potential (0.30 V) than OER (1.23 V) and the value-added 2,5-Furandicarboxylic acid (FDCA, one of the Top 12 bio-based building blocks) yield[5]. Although many advanced electrocatalysts have already been applied to drive the HER or HMFOR, it is still challenging to boost hydrogen production and yield FDCA with high selectivity simultaneously.

For the typical transition metal based electrocatalysts, the reaction mechanism of HMFOR can be divided in to the following two steps. Firstly, the active site with low-valence state is electrochemically oxidized to high-valence state by absorb OH^-. Then the formed oxidation state site chemically oxidizes the functional groups in HMF (activating and cleaving C–H/O–H bond) via hydride or hydrogen atom transfer[6,7]. Since the OH^- and HMF need to bind with oxygen vacancies, the electrocatalysts with moderate adsorption property toward OH^- can balance the competitive adsorption and achieve efficient HMFOR[8]. In earlier researches, single transition metals or compounds were used as the active component of HMFOR electrocatalysts, such as Ni_3N[9], Ni_2P[10] and Co_3O_4[11]. Although these components were susceptible to electrochemical oxidation, their immoderate adsorption properties toward OH^- limited the electrocatalytic performance, leading to higher onset potential ($>$ 1.35 V) and lower Faradic efficiency. Recently, heterostructure constructing strategy had been applied to adjust the electronic structure of the active site and to enhance the efficiency of HMFOR. For instance, Zhang et al. constructed the Co_9S_8–Ni_3S_2 for electrocatalytic HMFOR, in which the electron transferred from Ni_3S_2 to Co_9S_8, improving the adsorption of aldehyde group in HMF on Ni sites[12]. Besides, Wang et al. designed the CoP-CoOOH heterostructure for bifunctional HER and HMFOR electrocatalysis, where the CoP not only enhanced the charge transfer efficiency of as an electron donor during the reaction, but also served of HER active component to increase the electrocatalytic performance in the cathodic reaction[13]. However, the existing work on heterostructure construction mainly focused on boosting the adsorption performance of HMF molecule, and the relationship between their OH^- adsorption energy and electrocatalytic activity were rarely investigated in depth. Therefore, it was of great significance to develop heterostructure electrocatalyst with moderate hydroxide adsorption energy and evaluated their performance in HER-HMFOR bifunctional electrocatalysis.

Herein, a Ni_2P-$NiSe_2$ heterostructure aerogel (Ni-P-Se aerogel) was fabricated through facile reduction, freeze drying and anneal process. Specifically, $NiSe_2$ with cubic pyrite-type crystal structure possessed the surfaces that favor for surface reconstruction, which was an ideal component for anodic reaction. Moreover, the Ni_2P in the heterostructure not only transferred electrons to $NiSe_2$ and adjusted the excessive OH^- adsorption, but also provided excellent active substance toward HER. In addition, the aerogel structure with interconnect network skeleton offered abundant active sites and mass transfer pathway[14,15]. Benefit from these advantages, the Ni-P-Se aerogel exhibited high HER performance, high Faradaic efficiency toward HMFOR and significantly improved current density in two-electrode system.

2. MATERIAL AND METHOD

2.1 Materials and reagents

Nickle chloride hexahydrate ($NiCl_2{\cdot}6H_2O$, 99%), Sodium borohydride ($NaBH_4$, 98%) and Selenium (Se, 99.99%, powder, 100) were purchased from Adamas-beta. Ammonium hypophosphite ($NH_4H_2PO_2$, 97%), HMF (99.5%), FDCA (98%), DFF (98%), FFCA (98%) and HMFCA (98%) were purchased from Aladdin. Platinum-carbon (Pt/C, 20wt%) was purchased from Alfa Aesar.

2.2 Section of Introduction

In a typical preparation of Ni aerogel, 20 mL $NaBH_4$ (0.1 M) aqueous solution was quickly mixed with 10 mL $NiCl_2$ (0.05 M) aqueous solution. After 8 hours of resting, the Ni hydrogel was constructed at the bottom of the flask. The solvent in the hydrogel precursor was removed by 20 h freeze drying to get the Ni aerogel. To fabricate the Ni-P-Se aerogel, 20 mg of Ni aerogel, 40 mg of $NH_4H_2PO_2$ and 100 mg of Se powder were placed at three separate positions in porcelain boats, respectively, of which $NH_4H_2PO_2$ and Se powder were placed on the upstream side of the furnace. Then, the samples were annealed with Ar gas flowing at 250 °C and 400 °C for one hour each to synthesize the Ni-P-Se aerogel. Besides, the Ni-P and Ni-Se aerogels by annealing with only $NH_4H_2PO_2$ at 250 °C and only Se powder at 400 °C, respectively.

2.3 Characterizations

The morphology, microstructure and elemental mapping of Ni-P-Se aerogel and other prepared samples were analyzed by scanning electron microscope (SEM, SU8010) and transmission electron microscopy (TEM, Tecnai G2 F20). The crystal structures of obtained samples were characterized by powder X-ray diffraction (XRD, Rigaku Ultima IV). The chemical states of samples were manifested by X-ray photoelectron spectroscopy (XPS, Thermo ESCALAB 250XI) with an Al K X-ray source.

2.4 *Electrochemical measurements*

To prepare the working electode, 5.0 mg of aerogel powder was dispersed in the mixed solution with 0.25 mL ethanol, 0.25 mL deionized water and 20 µL of Nafion (5%) under sonication for 30 min to form homogeneous ink. Then, the prepared ink was all dropped on the surface of a piece of carbon paper (1 cm × 1 cm) followed by drying at 60 °C to achieve the loading amount of 5.0 $mg \cdot cm^{-2}$ for working electrode.

All the electrochemical properties of the samples were measured by a CHI 760 electrochemical workstation (CH Instruments, Inc., Shanghai) with three-electrodes system at room temperature, in which the graphite rod and Hg/HgO acted as counter, and reference electrodes, respectively. Electrocatalytic activities of cathodic reaction (HER) and anodic reactions (OER and HMFOR) were evaluated by linear-sweep voltammetry (LSV) in 1M KOH solution with/without 10 mM HMF at a scan rate of 5 $mV \cdot s^{-1}$ with 80% iR-correction. The potential ranges toward cathodic reaction and anodic reaction were -0.8 to -1.4 V and 0 to 0.8 V (vs. Hg/HgO), respectively. Further, the performance of two-electrodes system (HER+HMFOR and HER+OER) was also measured by LSV under the operating voltage from 1.0 to 2.0 V (without iR-correction). Electrochemical impedance spectroscopy (EIS) measurement was applied to evaluate the charge-transfer resistances of samples at a frequency range of 0.01 to 10^5 Hz. The testing voltages were set to -1.1 V and 0.7 V (vs. Hg/HgO) for cathodic and anodic reactions, respectively. Besides, the chronoamperometric test were used to measure the electrocatalytic stability and evaluate Faradic efficiency. For HER process, the voltage was set to achieve the initial current densities of 10 $mA \cdot cm^{-2}$ for 20 h. For the HMFOR process, the voltage was set as 1.40 V (vs. RHE) to drive the reaction.

2.5 *Theoretical calculation details*

Density functional theory (DFT) calculation was performed by DMol[3] code as implemented in Materials Studio. The generalized gradient approximation of Perdew-Burke-Ernzerhof (GGA-PBE) function was used to treat all the energy changes. The core treatment was effective core potentials (ECP) and the basis set was DNP v4.4. The k-point was set as 3×3×1 and the thickness of vacuum region was 15 Å. The OH^- adsorption energy and hydrogen adsorption Gibbs free energy (ΔG_{H^*}) were calaulated through the calculation.

2.6 *HPLC analysis*

The HMF and its oxidation products were analyzed by LC-10ADVP, Shimadzu. Specifically, 20 µL electrolyte was drawn out in the process of constant voltage electrolysis and diluted with deionized water (dilution ratio = 1:49), which was then analyzed by HPLC. A C18 column was used in the HPLC and the wavelength of the detector is 265 nm. Methanol and 5 mM ammonium formate aqueous solution were selected as the mobile phase, the ratio and flow rate were 3:7 and 1 mL/min, respectively. Calibration with reactants and products using commercial compounds. The conversion, selectivity, and Faradic efficiency were calculated based on published literature.

3. RESULTS AND DISCUSSION

3.1 *Synthesis and characterization of Ni-P-Se Aerogel*

The Ni-P-Se aerogel was fabricated through facile reduction, freeze drying and phosphating/selenizing with anneal process (**Scheme 1**). First of all, the Ni^{2+} from $NiCl_2$ aqueous solution was reduced by $NaBH_4$ to form Ni hydrogel. Herein, the hydrogen bubbles generated from the reactions served as the gas template and induced the construction of Ni hydrogel with porous networks skeleton[18]. Then, the Ni aerogel was produced by freeze drying to remove the solvent, and the obtained sample was phosphated and selenized to obtain the Ni-P-Se aerogels.

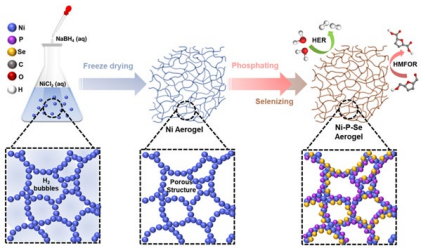

Scheme 1. Schematic illustration of the synthesis of Ni-P-Se aerogels

The SEM images in **Figure 1(a)** illustrated that the Ni aerogel possessed porous network structure composed by Ni nanoparticles. After annealing for phosphating and selenizing, the unique structure maintained well in Ni-P-Se aerogel (**Figure 1(b)**). It was noteworthy that the particles in the skeleton of Ni-P-Se aerogel presented slight agglomeration and recrystallization due to the conversion of components from Ni to phosphide or selenide[19]. The similar phenomena could be observed in Ni-P (**Figure 1(c)**) and Ni-Se (**Figure 1(d)**) aerogels, in which the changes were

more remarkable in the former. Moreover, the crystalline structures of Ni-P, Ni-Se and Ni-P-Se aerogels were investigated by powder XRD (**Figure 2(a)**). Obviously, two sets of characteristic peaks could be observed in the pattern of Ni-P-Se, which belonged to Ni_2P (PDF#97-010-5306) and $NiSe_2$ (PDF#97-004-0330), respectively. In addition, no characteristic peaks of metallic Ni were observed in the patterns of Ni-P-Se and Ni-P, indicating that the skeleton of the two aerogels were completely phosphated to Ni_2P by PH_3 (from $NH_4H_2PO_2$ decomposition)[20]. On the contrary, obvious characteristic peaks of metallic Ni were found in the

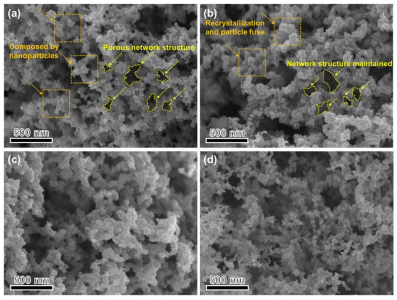

Figure 1. SEM image of (a) Ni aerogel, (b) Ni-P-Se aerogel, (c) Ni-P aerogel and (d) Ni-Se aerogel.

pattern of Ni-Se, demonstrating that Se vapor (from Se powder sublimation) could only selenize the surface of Ni aerogel. Furthermore, the construction of Ni_2P-$NiSe_2$ heterostructure in Ni-P-Se aerogel could be proved by the HRTEM image (**Figure 2(b)**), indicating that there were different two phases of Ni_2P and $NiSe_2$ on both sides of the heterointerface. In particular, the lattice fringes with interplanar distances of 0.292 and 0.225 nm were corresponded to the (200) crystal plane of $NiSe_2$ and (111) crystal plane of Ni_2P, respectively. In addition, the homogeneous distribution of Ni, P, and Se signals in elemental mapping (**Figure 2(c)**) further illustrated the successful synthesis of Ni_2P and $NiSe_2$ in the Ni-P-Se aerogel.

The XPS analysis was applied to comparably analyze the surface chemical composition and oxidation states of the Ni-P-Se aerogel and obtained samples. Upon the high-resolution spectrum of Ni 2p, except for the two satellite peaks at 861.2 and 878.0 eV, Ni-P-Se aerogel exhibited two major peaks at 852.9 and 870.3 eV, which were vested in Ni^{2+} and assigned to Ni $2p_{3/2}$ and Ni $2p_{1/2}$, respectively (the middle part of **Figure 3(a)**). The other two peaks at 856.3 and 874.2 eV were assigned to Ni^{3+}[21]. The similar peaks could be observed in the Ni 2p spectrum of Ni-Se (the upper part of **Figure 3(a)**) and Ni-P (the lower part of **Figure 3(a)**) aerogel. In particular, there were characteristic peaks of Ni^0 in the spectrum of Ni-Se, which was consistent with XRD and indicated the

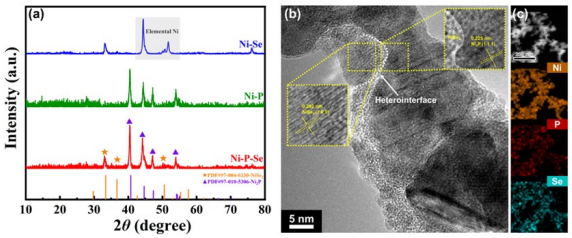

Figure 2. (a) XRD patterns of Ni-P, Ni-Se and Ni-P-Se aerogels. (b) HRTEM image of Ni-P-Se aerogel with lattice fringe of Ni_2P and $NiSe_2$ (c) STEM image of Ni-P-Se aerogel. and its corresponding elemental mapping of Ni, P, and Se.

partial selenizing on the surface. Compared with Ni-P and Ni-Se, the Ni^{2+} exhibited moderate valence states in the spectrum of Ni-P-Se (higher than Ni-P and lower than Ni-Se), which could provide appropriate OH^- adsorption property[19]. The high-resolution spectrum of P 2p (**Figure 3(b)**) included two sets of peaks, in which the peaks at 129.8 and 130.9 eV were the P $2p_{3/2}$ and P $2p_{1/2}$ for phosphide, and the peaks at 133.8 and 134.9 eV were the P $2p_{3/2}$ and P $2p_{1/2}$ for phosphate (mainly from the surface oxidation of phosphide)[22]. Due to the content of Ni_2P -$NiSe_2$ heterostructure, the peak of Se LMM could be observed in the Ni-P-Se spectrum, and the P 2p peak was significantly shifted compared to Ni-P. Besides, the Se 3d spectrum of Ni-P-Se was revealed in **Figure 3(c)**, where peaks at 54.2 and 55.1 eV were assigned to Se $3d_{5/2}$ and Se $3d_{3/2}$[23]. Similar with the P 2p, the Se 3d spectrum of Ni-P-Se presented positive shift compared to Ni-Se as well. Based on the results that discussed above, it was obvious that the electrons transferred from Ni_2P to $NiSe_2$ in the heterostructure (**Figure 3(d)**). To reveal the effects of charge transfer, basic DFT calculations were applied to evaluate the adsorption properties toward OH^- and H^-. The Ni_2P-$NiSe_2$ heterostructure exhibited moderate adsorption energy toward OH^- (0.93 eV), which was higher than that of Ni_2P (0.67 eV) and lower than that of $NiSe_2$ (1.19 eV), illustrating that the Ni-P-Se aerogel had the active sites that could efficiently catalyze HMFOR process (**Figure 3(e)**)[20]. Moreover, the Gibbs free energy of hydrogen adsorption (ΔG_{H^*}) for Ni_2P, $NiSe_2$ and the heterostructure were calculated to evaluate the potential HER performance (**Figure 3(f)**). In contrast, Ni_2P exhibited strong adsorption property toward H^* with relatively low ΔG_{H^*} of -0.28 eV, while the $NiSe_2$ was difficult to adsorb hydrogen for the high ΔG_{H^*} of 0.40 eV. The Ni_2P-$NiSe_2$ balanced the adsorption properties of the two ingredients and possessed the ΔG_{H^*} of 0.16 eV, which was close to the ideal state (0 eV)[24],

demonstrating that the Ni-P-Se aerogel had excellent application potential in HER as well.

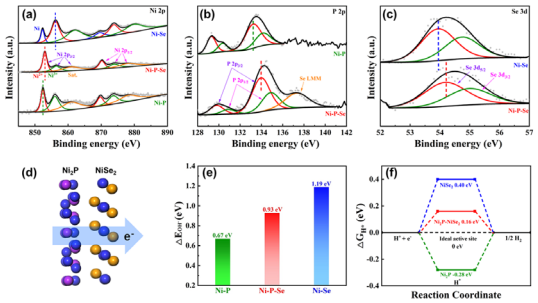

Figure 3. (a-c) High resolution Ni 2p, P 2p and Se 3d XPS spectra of Ni-P, Ni-Se and Ni-P-Se aerogels. (d) Electron transfer direction in the heterostructure (e-f) Free energy diagram of OH^-

3.2 Synthesis and characterization of Ni-P-Se Aerogel

The electrocatalytic hydrogen evolution reaction (HER) activities of prepared aerogels were investigated through LSV test in 1.0 M KOH under a scan rate of 5 $mV{\cdot}s^{-1}$ (**Figure 4(a)**). Ni-P-Se exhibited a lower overpotential of 68 mV at 10 $mA{\cdot}cm^{-2}$ than that of the Ni-P (94 mV at 10 $mA{\cdot}cm^{-2}$) and Ni-Se aerogels (145 mV at 10 $mA{\cdot}cm^{-2}$), which was consistent with DFT calculation and demonstrated the good HER activity in the heterostructure. Notably, the overpotential at 10 $mA{\cdot}cm^{-2}$ of Ni-P-Se was close to that of commercial Pt/C (34 mV), proving the potential for alternative noble metal electrocatalysts. The origin of excellent HER performance was analyzed by the Tafel slopes (**Figure 4(b)**). The Tafel slope value of Ni-P-Se was 56 $mV{\cdot}dec^{-1}$, which was close to that of Pt/C (34 $mV{\cdot}dec^{-1}$) and lower than that of $NiSe_2$-$CoSe_2$ (85 $mV{\cdot}dec^{-1}$), $Mo_{0.3}$-$NiSe_2$-$CoSe_2$ (113 $mV{\cdot}dec^{-1}$), indicating that the electrocatalytic process of Ni-P-Se followed Volmer-Heyrovsky and had favorable reaction kinetics[25]. Besides, the electrochemical impedance spectroscopy (EIS) measurement (**Figure 4(c)**) unraveled that the Ni-P-Se possessed lower charge transfer resistance (R_{ct}) than that of Ni-P and Ni-Se, suggesting that the heterostructure enhanced charge transfer between Ni_2P and $NiSe_2$. In addition , the current density retained 96% of the initial value after 20 hours (**Figure 4(d)**)., demonstrating the Ni-P-Se aerogel possess good stability

To prove the superiority of Ni-P-Se in anodic reaction , the OER and HMFOR performance were tested through LSV (**Figure 5(a) and Figure 5(b)**). Obviously, the Ni-P-Se aerogel exhibited lower onset potential of 1.30 V than that of Ni-P and Ni-Se, demonstrating that the heterostructure of Ni_2P-$NiSe_2$ provided favorable active site for anodic oxidation. It was worth mentioning that

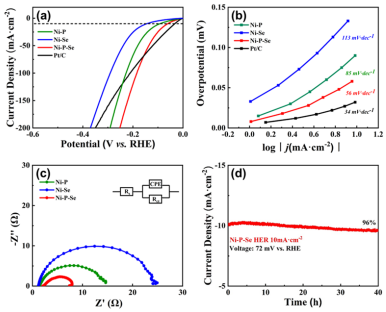

Figure 4. (a-b) Polarization LSV curves and Tafel slopes of Ni-P, Ni-Se, Ni-P-Se aerogels and Pt/C toward HER in 1.0M KOH. (c) EIS measurement of Ni-P, Ni-Se and Ni-P-Se aerogels toward HER. (d) Chronoamperometric measurement of Ni-P-Se aerogel toward HER with the initial current densities of 10 $mA{\cdot}cm^{-2}$

there was no significant difference in the onset potential of Ni-P-Se toward OER and HMFOR, but the current density at 1.4V is significantly increased after the addition of 10 mM HMF. Moreover, the EIS measurement (**Figure 5(c)**) presented that the Ni-P-Se possessed lower R_{ct} than that of Ni-Pand Ni-Se, indicating that the enhancement of charge transfer that provided by heterostructure also exist in anodic reaction. Besides, the Ni-Se aerogel exhibited lower R_{ct} than that of Ni-P, which was different from the trend in HER, illustrating that Ni_2P and $NiSe_2$ were suitable for cathodic and anodic reactions, respectively[2]. In addition, to illustrate the significance of HMFOR as a substitute for OER, a two-electrode system with Ni-P-Se aerogel was constructed. It could be demonstrated that when HER was coupled with HMFOR, the current density at 1.5 V is enhanced by 102 mA compared to water splitting (HER and OER), indicating that the lower voltage requirement of HMFOR enhanced the reaction efficiency of hydrogen generation.

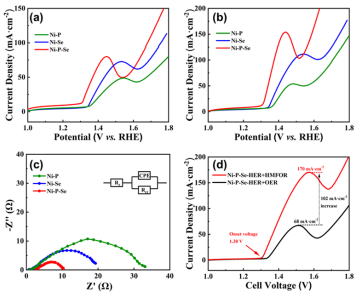

Figure 5. (a-b) Polarization LSV curves of Ni-P, Ni-Se and Ni-P-Se aerogels toward OER and HMFOR in 1.0M KOH. (c) EIS measurement of Ni-P, Ni-Se and Ni-P-Se aerogels toward anodic reaction. (d) Polarization LSV curves of Ni-P-Se for two electrodes system.

As it was shown in **Figure 6(a)**, two reaction pathways for HMF oxidation, including the initial alcohol hydroxyl oxidation to DFF and aldehyde oxidation to HMFCA[26]. The main condition that controled the reaction path was the pH of electrolyte, and for the system we used, the reaction process followed the path of HMFCA formation. The chronoamperometric test result of Ni-P-Se toward HMFOR was shown in **Figure 6(b)**. As the reaction proceeded, the concentration of HMF decreased, and the current density decreases to near 0 after two hours. **Figure 6(c)** and **Figure 6(d)** demonstrated the chromatogram and concentration change curves of HMFOR with time, respectively. Based on the results, the HMF conversion, selectivity of FDCA, and Faradic efficiency were 99.7 %, 99.2 %, and 97.4 %, respectively. In addition, after repeated the chronoamperometric test for four times, the Faraday efficiency of Ni-P-Se can still maintain more than 87%, indicating the good stability for electrocatalytic HMFOR.

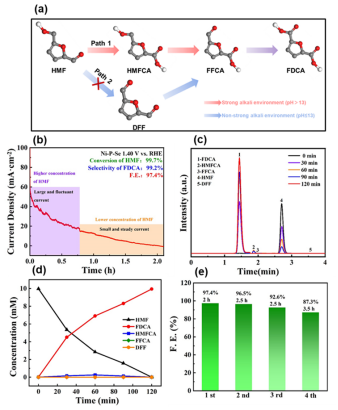

Figure 6. (a) The oxidation path of HMF. (b) The chronoamperometric test result of Ni-P-Se toward HMFOR (c) The chromatogram of HMFOR. (d)The concentrations change curves of HMFOR. (e) Faradic efficiency of Ni-P-Se for four times HMFOR test.

4. CONCLUSIONS

In summary, we designed and synthesized a novel Ni-P-Se aerogel via facile gelation, freeze drying and annealing. The Ni-P-Se aerogel exhibited splendid performance toward both cathodic and anodic reaction, which could be proved by the low overpotential of HER (68 mV at 10 mA·cm^{-2}), low onset potential of oxidation (1.30 V) and high Faradic efficiency of HMFOR (97.4% at 1.40 V). Compared to OER, the current density of two-electrode system coupled with HMFOR revealed 102 mA·cm-2 increase at 1.50 V. Based on the results of characterization and DFT calculations, it was clear that this excellent performance was not only from the intrinsic activity of Ni_2P and $NiSe_2$ for cathodic and anodic reactions, but also from the optimal electronic structure and suitable adsorption energy for H* and OH^- at the heterointerface. Besides, the unique porous network structure of aerogel provided abundant active sites and mass transfer pathways, enhancing the electrocatalytic properties. In conclusion, our work afforded a new and facile approach to construct bifunctional electrocatalyst for efficient green hydrogen generation and value-added FDCA production.

ACKNOWLEDGEMENT

We gratefully thank for the National Natural Science Foundation of China (Nos.22278431, Nos.21776302).

DECLARATION OF INTEREST STATEMENT

The authors declare that they have no known competing financial interests or personal relationships that could have appeared to influence the work reported in this paper. All authors read and approved the final manuscript.

REFERENCE

[1] Z. Wang, S. Li, Z. Jin, Z. Li, Q. Liu, K. Zhang, Oil and gas pathway to net-zero: Review and outlook, Energy Strateg. Rev. 45 (2023) 101048.

[2] X. Peng, Y. Yan, X. Jin, C. Huang, W. Jin, B. Gao, P.K. Chu, Recent advance and prospectives of electrocatalysts based on transition metal selenides for efficient water splitting, Nano Energy. 78 (2020) 105234.

[3] J. Zhu, L. Hu, P. Zhao, L.Y.S. Lee, K.Y. Wong, Recent Advances in Electrocatalytic Hydrogen Evolution Using Nanoparticles, Chem. Rev. 120 (2020) 851–918.

[4] X. Wu, Y. Wang, Z.S. Wu, Design principle of electrocatalysts for the electrooxidation of organics, Chem. 8 (2022) 2594–2629.

[5] Y. Kwon, K.J.P. Schouten, J.C. Van Der Waal, E. De Jong, M.T.M. Koper, Electrocatalytic Conversion of Furanic Compounds, ACS Catal. 6 (2016) 6704–6717.

[6] W. Chen, C. Xie, Y. Wang, Y. Zou, C.L. Dong, Y.C. Huang, Z. Xiao, Z. Wei, S. Du, C. Chen, B. Zhou, J. Ma, S. Wang, Activity Origins and Design Principles of Nickel-Based Catalysts for Nucleophile Electrooxidation, Chem. 6 (2020) 2974–2993.

[7] B.J. Taitt, D.H. Nam, K.S. Choi, A Comparative Study of Nickel, Cobalt, and Iron Oxyhydroxide Anodes for the Electrochemical Oxidation of 5-Hydroxymethylfurfural to 2,5-Furandicarboxylic Acid, ACS Catal. 9 (2019) 660–670.

[8] Y. Yang, T. Mu, Electrochemical oxidation of biomass derived 5-hydroxymethylfurfural (HMF): pathway, mechanism, catalysts and coupling reactions, Green Chem. 23 (2021) 4228–4254.

[9] N. Zhang, Y. Zou, L. Tao, W. Chen, L. Zhou, Z. Liu, B. Zhou, G. Huang, H. Lin, S. Wang, Electrochemical Oxidation of 5-

Hydroxymethylfurfural on Nickel Nitride/Carbon Nanosheets: Reaction Pathway Determined by In Situ Sum Frequency Generation Vibrational Spectroscopy, Angew. Chemie-Int. Ed. 58 (2019) 15895–15903.
[10] B. You, N. Jiang, X. Liu, Y. Sun, Simultaneous H2Generation and Biomass Upgrading in Water by an Efficient Noble-Metal-Free Bifunctional Electrocatalyst, Angew. Chemie - Int. Ed. 55 (2016) 9913–9917.
[11] Z. Zhou, C. Chen, M. Gao, B. Xia, J. Zhang, In situ anchoring of a Co3O4 nanowire on nickel foam: An outstanding bifunctional catalyst for energy-saving simultaneous reactions, Green Chem. 21 (2019) 6699–6706.
[12] Y. Zhang, Z. Xue, X. Zhao, B. Zhang, T. Mu, Controllable and facile preparation of Co9S8-Ni3S2heterostructures embedded with N,S,O-tri-doped carbon for electrocatalytic oxidation of 5-hydroxymethylfurfural, Green Chem. 24 (2022) 1721–1731.
[13] H. Wang, Y. Zhou, S. Tao, CoP-CoOOH heterojunction with modulating interfacial electronic structure: A robust biomass-upgrading electrocatalyst, Appl. Catal. B Environ. 315 (2022) 121588.
[14] H. Liu, F. Yang, F. Chen, S. Che, N. Chen, C. Xu, N. Wu, W. Wei, Y. Li, Bimetallic Ni-Co selenide heterostructure aerogel for highly efficient overall water splitting, Mater. Chem. Front. (2023) 1365–1373.
[15] H. Liu, F. Yang, F. Chen, S. Che, N. Chen, S. Sun, N. Ta, Y. Sun, N. Wu, Y. Sun, Y. Li, Interface and electronic structure regulation of Mo-doped NiSe2-CoSe2 heterostructure aerogel for efficient overall water splitting, J. Colloid Interface Sci. 640 (2023) 1040–1051.
[16] K. Deng, T. Ren, Y. Xu, S. Liu, Z. Dai, Z. Wang, X. Li, L. Wang, H. Wang, Transition metal M (M = Co, Ni, and Fe) and boron co-modulation in Rh-based aerogels for highly efficient and pH-universal hydrogen evolution electrocatalysis, J. Mater. Chem. A. 8 (2020) 5595–5600.
[17] A.A. Dubale, Y. Zheng, H. Wang, R. Hübner, Y. Li, J. Yang, J. Zhang, N.K. Sethi, L. He, Z. Zheng, W. Liu, High-Performance Bismuth-Doped Nickel Aerogel Electrocatalyst for the Methanol Oxidation Reaction, Angew. Chemie - Int. Ed. 59 (2020) 13891–13899.
[18] L. Liu, L.X. Chen, A.J. Wang, J. Yuan, L. Shen, J.J. Feng, Hydrogen bubbles template-directed synthesis of self-supported AuPt nanowire networks for improved ethanol oxidation and oxygen reduction reactions, Int. J. Hydrogen Energy. 41 (2016) 8871–8880.
[19] C. Liu, T. Gong, J. Zhang, X. Zheng, J. Mao, H. Liu, Y. Li, Q. Hao, Engineering Ni2P-NiSe2 heterostructure interface for highly efficient alkaline hydrogen evolution, Appl. Catal. B Environ. 262 (2020) 1–8.
[20] X. Yun, T. Lu, R. Zhou, Z. Lu, J. Li, Y. Zhu, Heterostructured NiSe 2 / CoSe 2 hollow microspheres as battery-type cathode for hybrid supercapacitors : Electrochemical kinetics and energy storage mechanism, Chem. Eng. J. 426 (2021) 131328.
[21] G. Wang, W. Chen, G. Chen, J. Huang, C. Song, D. Chen, Y. Du, C. Li, K.K. Ostrikov, Trimetallic Mo–Ni–Co selenides nanorod electrocatalysts for highly-efficient and ultra-stable hydrogen evolution, Nano Energy. 71 (2020) 104637.
[22] J. Lin, Y. Yan, C. Li, X. Si, H. Wang, J. Qi, Bifunctional Electrocatalysts Based on Mo ‐ Doped NiCoP Nanosheet Arrays for Overall Water Splitting, Nano-Micro Lett. 11 (2019) 1–11.
[23] X. Zhang, Y. Ding, G. Wu, X. Du, CoSe2@NiSe2 nanoarray as better and efficient electrocatalyst for overall water splitting, Int. J. Hydrogen Energy. 45 (2020) 30611–30621. https://doi.org/10.1016/j.ijhydene.2020.08.096.
[24] B. Jansi Rani, G. Ravi, R. Yuvakkumar, B. Saravanakumar, M. Thambidurai, C. Dang, D. Velauthapillai, CoNiSe2Nanostructures for Clean Energy Production, ACS Omega. 5 (2020) 14702–14710.
[25] D. Chen, Z. Xu, W. Chen, G. Chen, J. Huang, J. Huang, C. Song, C. Li, K. (Ken) Ostrikov, Just add water to split water: ultrahigh-performance bifunctional electrocatalysts fabricated using eco-friendly heterointerfacing of NiCo diselenides, J. Mater. Chem. A. 8 (2020) 12035–12044.
[26] Y. Song, W. Xie, Y. Song, H. Li, S. Li, S. Jiang, J.Y. Lee, M. Shao, Bifunctional integrated electrode for high-efficient hydrogen production coupled with 5-hydroxymethylfurfural oxidation, Appl. Catal. B Environ. 312 (2022) 121400.